Pertanika J. Sci. & Technol. 29 (1): 533 - 545 (2021)

PERTANIKA JOURNALS

SCIENCE & TECHNOLOGY

Journal homepage: http://www.pertanika.upm.edu.my/

Algorithm for B-scan Image Reconstruction in Optical Coherence Tomography

Kranti Patil[1], Anurag Mahajan[1]*, Balamurugan Subramani[2], Arulmozhivarman Pachiyappan[3] and Roshan Makkar[4]

[1]Department of Electronics and Telecommunication, Symbiosis Institute of Technology, Symbiosis International(Deemed University), (SIU) Lavale, Pune, (Maharashtra), India
[2]Department of Instrumentation, School of Electrical Engineering, VIT, Vellore, Tamil Nadu, India
[3]School of Electrical Engineering, VIT, Vellore, Tamil Nadu, India
[4]Department of Photonics, Society of Applied Microwave Electronics Engineering and Research (SAMEER) Mumbai, Maharashtra, India

ABSTRACT

Optical coherence tomography (OCT) is an evolving medical imaging technology that offers in vivo cross-sectional, sub-surface images in real-time. OCT has become popular in the medical as well as non-medical fields. The technique extensively uses for food industry, dentistry, dermatology, and ophthalmology. The technique is non-invasive and works on the Michelson interferometry principle, i.e., dependent on back reflections of the signal and its interference. The objective is to develop an algorithm for signal processing to construct an OCT image and then to enhance the quality of the image using image processing techniques like filtering. The image construction was primarily based on the Fourier transform (FT) of the dataset obtained by data acquisition. This FT could be performed rapidly with the extensively used algorithm of fast Fourier transform (FFT). The depth-wise information could be extracted from each A-scan, i.e., axial scan and also the B-scan was obtained from the A-scan to see the structure of sample. The maximum penetration depth achieved with proposed system was 2.82mm for 1024 data points. First and second layer of leaf were getting at thickness of 1mm and 1.6mm, respectively. A-scans for Human fingertip gave its first, second and third layer was at a

ARTICLE INFO

Article history:
Received: 09 October 2020
Accepted: 16 November 2020
Published: 22 January 2021

DOI: https://doi.org/10.47836/pjst.29.1.28

E-mail addresses:
krantipatil1111@gmail.com (Kranti Patil)
anurag.mahajan@sitpune.edu.in (Anurag Mahajan)
sbalamurugan@vit.ac.in (Balamurugan Subramani)
parulmozhivarman@vit.ac.in (Arulmozhivarman Pachiyappan)
roshan@sameer.gov.in (Roshan Makkar)
* Corresponding author

ISSN: 0128-7680
e-ISSN: 2231-8526

thickness of 0.75mm, 0.9mm and 1.6mm, respectively. A-scans for foam sheet gave its first, second and third layer was at a thickness of 0.6mm, 0.75mm, and 0.85mm, respectively.

Keywords: A-scan, b-scan, depth profile, filtering, image processing, optical coherence tomography (OCT), signal processing

INTRODUCTION

With The rapid expansion in the field of medical imaging technologies, a huge amount of biomedical image data can be collected by several biomedical techniques like X-ray, Magnetic Resonance Imaging (MRI), 3D ultrasound, and Optical Coherence Tomography (OCT) (Lee et al., 2019; Drexler & Fujimoto, 2008). Three-dimensional medical modalities can examine numerous features of biological features, such as blood flow, structural information of organs, and molecular content, which gives a crisp of the scanned object (Zhang et al., 2018). The OCT system is also used to analyze the final B-scan image and get to a medical conclusion. The main analysis is on the retinal layers (Schönfeldt-Lecuona et al., 2020, Chua et al., 2020) and neural layer (Liu et al., 2020) to get the structural information.

The principle used for OCT system is Michelson Interferometry (Panta et al., 2019). A light source of low coherence is used in Michelson Interferometer, as displayed in Figure 1. As shown in Figure 1, the source of light beam having broadband spectrum is divided in two portions i.e., sample and reference arm by the beam splitter (Tomlins & Wang, 2005). Sample and reference arm reflect the signal which forms the pattern of interference and this pattern is detected by the spectrometer in which photocurrent of the pattern is measured by using the line scanning camera (Lee et al., 2020).

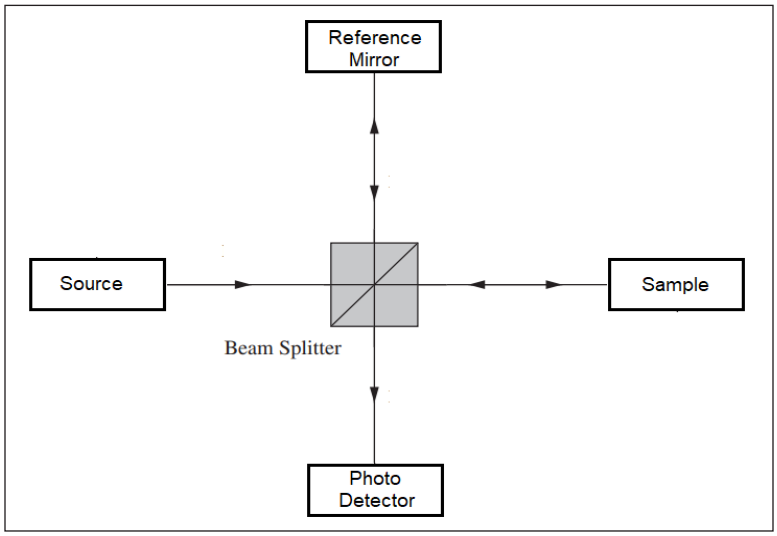

Figure 1. Principle of Michelson interferometer

The light falls on line scanning camera where the photocurrent of light is detected with the array of pixels to give the intensity corresponding to each wavelength in the bandwidth. This data is then taken for the signal processing for the image formation (Tang et al., 2018). Figure 1 describes the working principle of Michelson Interferometer, where half-silvered beam splitter is used (Kim et al., 2018; Lee et al., 2011).

Bhatia et al. (2016) described the core of the OCT systems and implemented the spectral-domain OCT(SD-OCT). The detected signal from the OCT gives three terms of getting in the data, which were constant term, autocorrelation and cross-correlation (Bhatia et al., 2016). The different applications of OCT in clinical and non-clinical fields are discovered. The spectrometer gives information about one-dimensional data by taking the interference signal as an input (Fujimoto & Swanson, 2016; Patil et al., 2020). The system uses the signal processing algorithm, which has the blocks of background removal, resampling, FFT and DC removal (Choudhari et al., 2017). The system uses the wavelength of 840nm with 40nm bandwidth and getting the depth profile which gives imaging depth of 0.5mm. Zhang et al. (2018) implemented the swept-source OCT (SS-OCT) for imaging the choriocapillaris and associated flow voids. The system works on the wavelength of 1060nm and bandwidth of 100nm. The final images of choriocapillaris give information regarding the diseases and the response of the body to therapies. Petrov et al. (2016) applied the short time Fourier transforms in the signal processing, using the window and this window slid along the time series. This algorithm takes more time to execute as it is having more point FFT, also we see the maximum penetration depth is not much and if we want to image the tissue to certain depth we need more penetration depth (Petrov et al., 2016).

From the literature survey, we have found that the imaging depth in the existing systems is typically in the range of 1-2 mm, hence there is a scope of improvement in the imaging depth. Therefore, in this paper, we proposed the system which worked on the wavelength of 840nm and bandwidth of 64nm and developed the algorithm to increase the maximum penetration depth. Also, in OCT, the speckle noise gets added to the final B-scan images. This noise is reduced by applying some image processing techniques so as to improve the quality of the image for the better interpretation.

MATERIALS AND METHODS

Signal Processing in OCT

The data acquisition process was executed by implementing Spectral-domain OCT (SD-OCT). In order to obtain the final OCT images the fundamental blocks were used as shown in Figure 2.

In every system some background noise gets added in the system due to reflections of room light and electronic devices (Rawat & Gaikwad, 2014). This background noise is an important factor in image formation as it disturbs the image, hence it needs to be removed.

The output of the Michelson interference is nothing but the interference pattern in the form of fringes. The interference pattern has the optical light; this optical intensity is measured by the spectrometer (Lee et al., 2011). As for image formation FFT is taken and for which the data must be evenly sampled in wavenumber space, for this resampling and interpolation blocks are followed. The image objects frequently used in OCT comprise of dispersive media, where the speed for optical frequencies are not the same as for different mediums speed is different. The individual reflections form the sample, and those reflections from specific scatters not likely to form the point images, rather they blurred by dispersion. Due to mismatch between the sample and reference arm of the interferometer the non-linear phase, which is dependent on frequency is introduced and by cancelling this phase, the dispersion can be compensated.

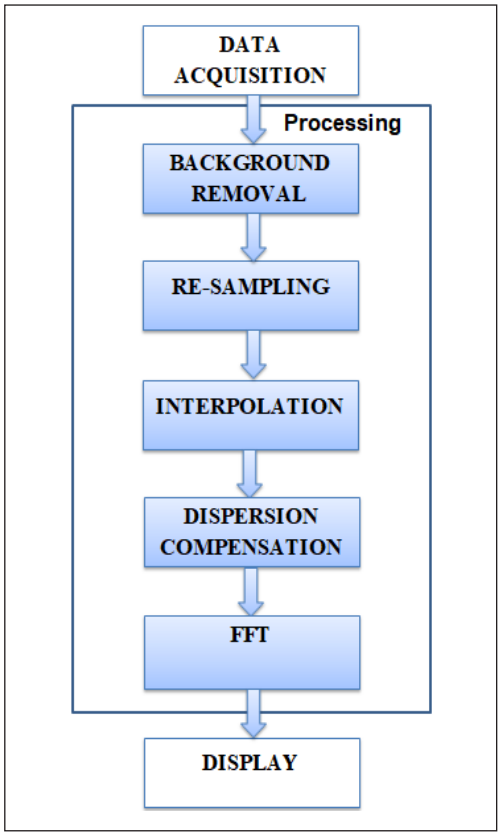

Figure 2. Signal processing algorithm

The phase correction is can be calculated as in Equation 1 (Ali & parlapalli, 2010)

$$\varphi(\omega) = -[(b * n^2) + (c * n^3)] \quad (1)$$

Where b and c are linear constants; n is a vector of linear elements from -1 to 1.

This phase which is equal and opposite to the physical wavelength-dependent path length shift is multiplied to each element of the spectrum in order to compensate the dispersion (Marks et al., 2002). The FFT is taken in the last to get the depth resolved profile (McKeown, 2010).

Formation of B-scan Image

The mechanism involves scanning the sample along the optical axis. One dimensional scanning is performed in the *Z*-direction, and it is known as the axial scanning or A-scan. One dimensional scanning can only give information about the single point of the sample. The two-dimensional scanning can be obtained by combining the multiple axial scans. The

two-dimensional scan is also known as B-scan. A scan includes point scanning, whereas B scanning involves scanning the entire surface. The flowchart for getting B-scan is as shown in Figure 3. It follows the flow from acquisition of the data from the experimental setup of the OCT. The single point data is taken to signal processing algorithm to form a depth profile of that particular point. As the data can be processed and 512 axial scans are formed. Now for the formations of the B-scan image all these 512 A-scans are stacked sequentially to get the final OCT image

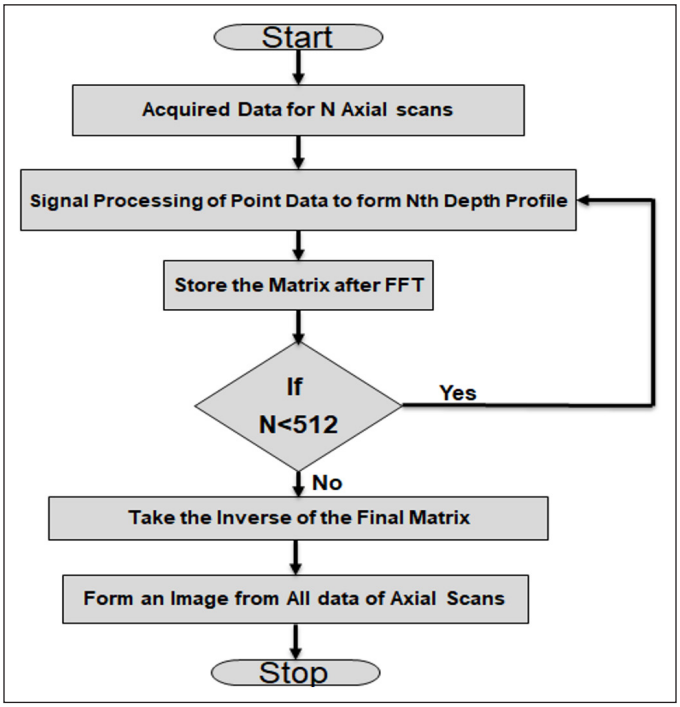

Figure 3. Flow chart for B-scan formation

Image Processing in OCT

Low-coherence interferometry is used in the OCT imaging, which introduces some speckle noise in the images, and this speckle-noise is the granular noise, seen as black and white spots on the images (Frosz et al., 2001). This speckle noise is a ubiquitous artifact that limits the interpretation as it profoundly affects the quality, contrast of the image and makes the difficulties in analyzing the exceptional features and structures. The back reflections of the incident light generates a signal which carries speckle, while due to scattering of photons in forwarding and backward direction generates the signal-degrading speckle (Petrov et al., 2016). The speckle is visible as grainy structures which blurs the details of the structural image (Murakami & Ogawa, 2018). As this speckle-noise needs to be removed but removing speckle noise removes some useful information also hence the special care should be taken.

Therefore, it is crucial to take out the speckle noise with care and for better interpretation, image enhancement and filtering techniques are used. Here the median filtering gives the best results from other filtering techniques.

Median Filtering

The median filter is an order statistics filter. This filtering technique is used to eliminate the noise by preserving the sharp edges in the images. This technique comes under non-linear filtering techniques. The impulse noise is also eliminated by the average filtering, in which centre pixel is replaced with average of neighbouring pixels, but in this filtering technique, the fine details of the image are not preserved and hence the loss of information occurs. While in the case of median filtering, the centre pixel is replaced by the median of the neighbouring pixel. Median filters are one-dimensional as well as two- dimensional. The results of two-dimensional median filters are better than that of one-dimensional median filter. The results are shown in the results section.

RESULTS AND DISCUSSION

We had acquired the data from the SD-OCT system setup for three different samples of a leaf, human fingertip, and foam sheet. The dataset was in terms of the intensities and the respective wavelengths. The data set was then applied to the several steps of signal processing algorithm like background subtraction, resampling interpolation, dispersion compensation and FFT. The Signal Processing Algorithm gives the Depth profile of the sample, i.e., Axial scan (A-scan). This A-scan was obtained after processing algorithm on the dataset. The dataset in our case was 512×1024, i.e., a total of 512 A-scans each having 1024 pixels. The depth profiles for samples like a leaf, human fingertip and foam sheet are given in the following part.

Each A-scan gives the layer-wise depth information about the thickness. The proposed system provides maximum penetration depth at 2.82mm for each sample only differing in the position of the peaks which is shown in Figures 4, 5 and 6. As each sample had 512 A-scan in our case and four of them are shown for each sample. The first A-scan from Figure 4 gave information that the first and second layer were getting at thickness of 1mm and 1.6mm, respectively. Likewise, the depth information could be extracted from every A-scan.

A-scans for Human fingertip is shown in Figure 5. The information taken out from the first A-scan is the first, second and third layer is getting at a thickness of 0.75mm, 0.9mm and 1.6mm, respectively.

Another sample was the foam sheet. Foam sheet having multiple layers can be seen by the A-scans shown in Figure 6. Also, for foam sheet, the layers are different at each point. The layers are coming at 0.6mm, 0.75mm and 0.85mm thickness.

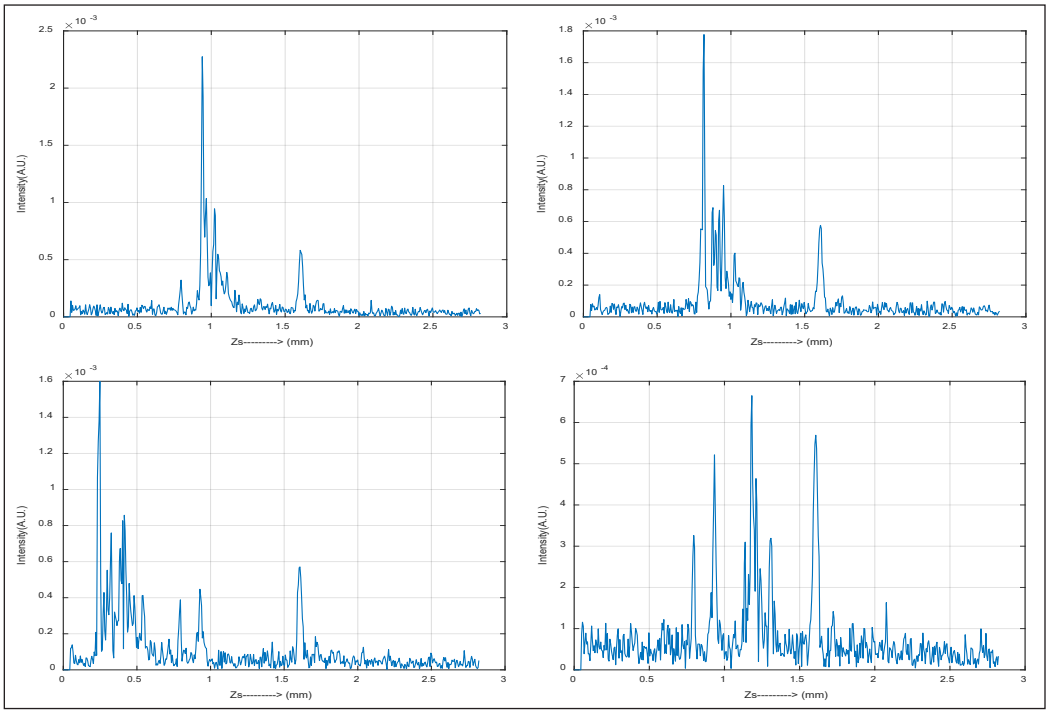

Figure 4. A-scans of leaf

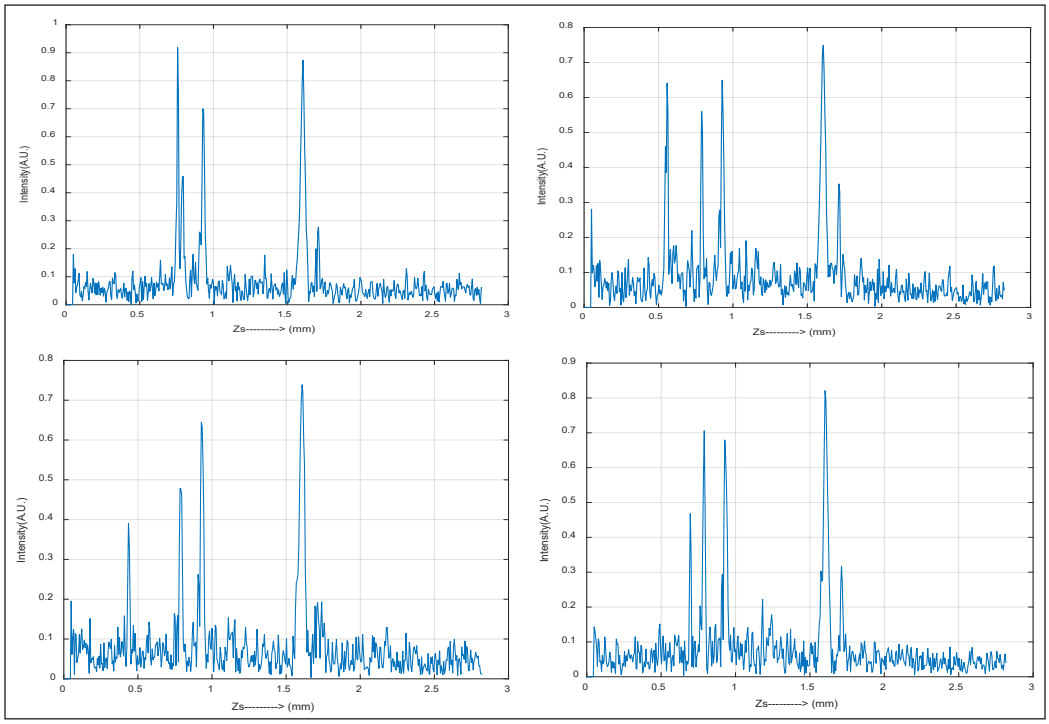

Figure 5. A-scans of human fingertip

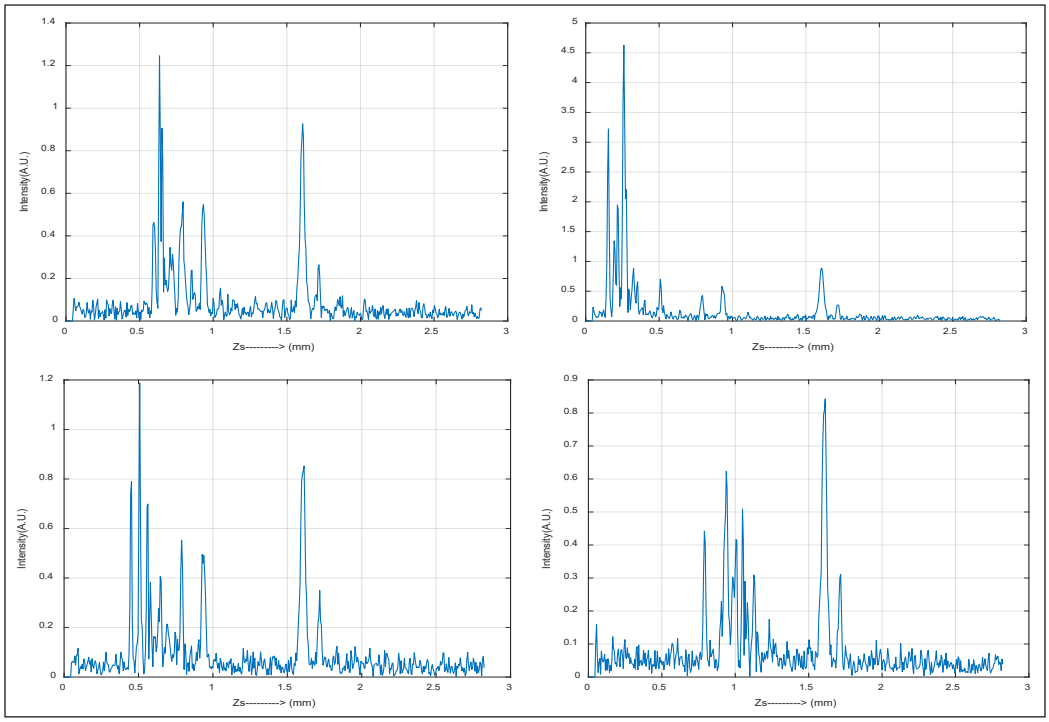

Figure 6. A-scans of foam sheet

Table 1
Comparison with existing systems

Year	Maximum Depth	Number of pixels per A-scan
Bhatia et al., 2016	0.5 nm	128
Lee et al., 2019	2.6 mm	1024
Zhang et al., 2018	3 mm	2048
Patil et al., 2020	2.75mm	1024
Proposed	2.82mm	1024

From Table 1, it is clear that the proposed system gave the maximum penetration depth as compared to the existing system for the same number of data points. As for imaging the tissues or some sample, the maximum penetration depth should be as high as possible with the minimum number of pixels, as with pixel numbers, the complexity increases. Now to form the B-scan image we had arranged all these 512 depth profiles, i.e., A-scans in a sequential manner followed by Figure 3 and the B-scan images as shown in Figure 7.

This 2-dimensional, i.e., B-scan image gives the structural information about the sample. The above B-scan is of a leaf, and the deep middle part indicates the axis of the leaf. Likewise, more information can be extracted after the feature extraction technique. In similar ways, B-scan for human fingertip, foam sheet and stack tape were obtained and

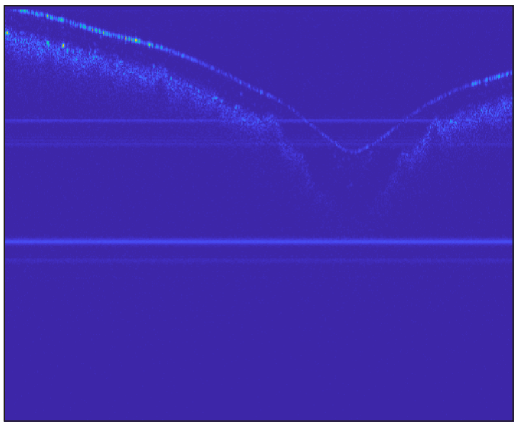

Figure 7. B-scan of leaf (512×512)

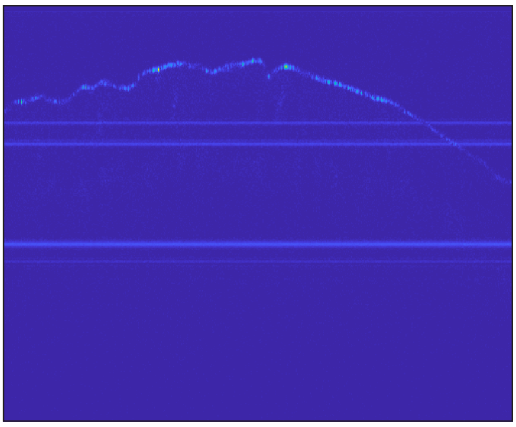

Figure 8. B-scan image of human fingertip (512×512)

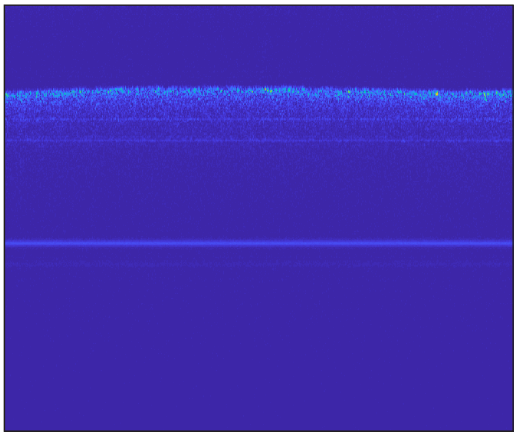

Figure 9. B-Scan of foam sheet (512×512)

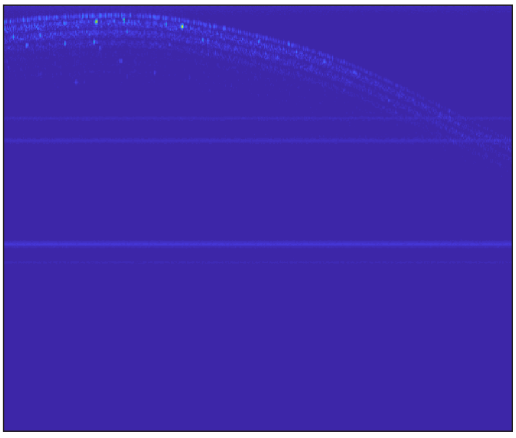

Figure 10. B-Scan of stack of tape (512×512)

shown in Figures 8, 9 and 10, respectively. Also, in every B-scan there are some horizontal lines, these horizontal lines are due to the system and those can be ignored.

The above B-scan in Figure 8 is of the human fingertip and having the pixel size 512×512. The image shows the skin layers of the fingertip. The above B-scan is of the foam sheet, and it has multiple layers at each point. B-scan image of the stack tape is shown in Figure 10.

These B-scan images can be enhanced by using some image processing technique like filtering. The impact of different filters on the B-scan image is studied by applying different filtering techniques on the sample image. The image quality is improved more with two-dimensional median filtering amongst the other techniques like average and 1-D filtering. The speckle noise is reduced to some amount after using the filtering technique. The results after filtering are shown in Figures 11 to 14.

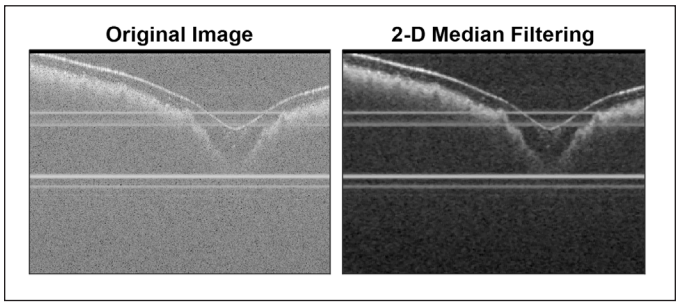

Figure 11. Filtering result for leaf (512×512)

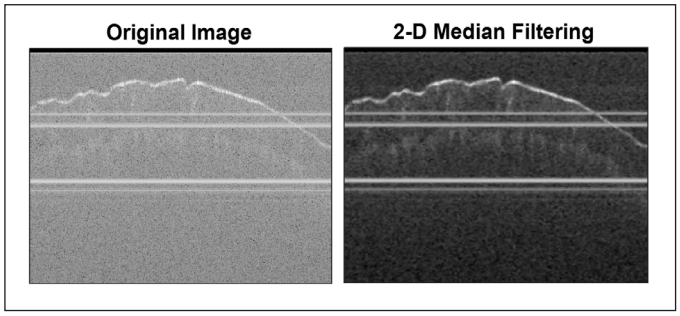

Figure 12. Filtering result for human fingertip (512×512)

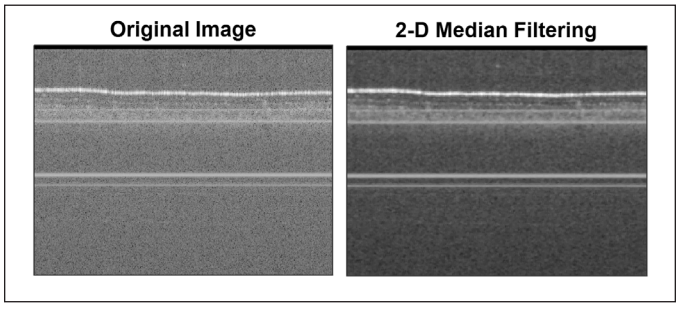

Figure 13. Filtering result for foam sheet (512×512)

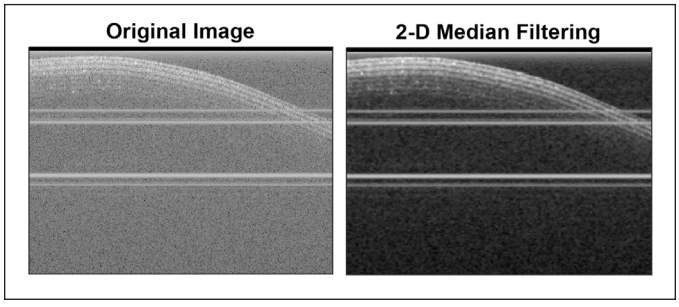

Figure 14. Filtering result for stack of tape (512×512)

The median filtering is applied in two ways, i.e., 1-dimensional and 2-dimensional. The results are better with 2-dimensional median filtering as the method gives the best quality images amongst other filtering technique.

CONCLUSIONS AND FUTURE SCOPE

The dataset is obtained by SD-OCT system setup for three different samples like human fingertip, leaf, and foam sheet. The signal processing algorithm is executed on the MATLAB to get the depth profile at each point. Thus, for every sample, 512 axial scans are collected, and each of A-scan is consisted of 1024 pixels, by combining these entire axial scans, B-scan image is formed. The maximum penetration depth calculated from the axial scan is 2.82mm for 1024 data points. The image processing technique of filtering applied on the sample image to see the impact of different filters on the B-scan image. The image quality is improved more with two-dimensional median filtering amongst all other techniques.

In future work, the detailed structural information can be obtained by feature extraction techniques and by applying some artificial intelligence (Kapoor et al., 2019) and machine learning algorithm, the automated analysis can be obtained.

ACKNOWLEDGEMENT

Mr. Kranti Patil is thankful to Director-General for the opportunity to work on the live project, Photonics Division, SAMEER, IIT Bombay for providing the necessary equipment required to carry out this work. Authors would like to thank Department of Science and Technology (DST) for funding support for the project sanction number IDP/MED/53/2016 under Biomedical Device and Technology (BDTD).

REFERENCES

Ali, M., & Parlapalli, R. (2010). *Signal processing overview of optical coherence tomography systems for medical imaging* (SPRABB9–June). Texas Instruments. Retrieved October 09, 2020, from https://www.researchgate.net/publication/268356516_Signal_Processing_Overview_of_Optical_Coherence_Tomography_Systems_for_Medical_Imaging/link/54eb3d620cf25ba91c8652df/download}

Bhatia, P., Choudhari, S., Rodrigues, A., Patil, M., & Makkar, R. (2016, March 23-25). High resolution imaging system using spectral domain Optical Coherence Tomography using NIR source. In *2016 International Conference on Wireless Communications, Signal Processing and Networking (WiSPNET)* (pp. 2212-2216). Chennai, India. doi: 10.1109/WiSPNET.2016.7566535

Choudhari, S., Patil, M., & Makkar, R. (2017). Modelling for spectral domain optical coherence tomography (SD-OCT) system. In I. Bhattacharya, S. Chakrabarti, H. Reehal & V. Lakshminarayanan (Eds.), *Advances in Optical Science and Engineering* (pp. 591-597). Singapore: Springer. doi: https://doi.org/10.1007/978-981-10-3908-9_74

Chua, J., Sim, R., Tan, B., Wong, D., Yao, X., Liu, X., ... & Schmetterer, L. (2020). Optical coherence tomography angiography in diabetes and diabetic retinopathy. *Journal of Clinical Medicine*, *9*(6), 1-28. doi: https://doi.org/10.3390/jcm9061723

Drexler, W., & Fujimoto, J. G. (2008). *OCT Technology and Applications. Biomedical Engineering.* Heidelberg, Germany: Springer. doi: 10.1007/978-3-540-77550-8

Frosz, M. H., Juhl, M., & Lang, M. H. (2001). *Optical coherence tomography: System design and noise analysis*. Roskilde, Denmark: Risø National Laboratory.

Fujimoto, J., & Swanson, E. (2016). The development, commercialization, and impact of optical coherence tomography. *Investigative Ophthalmology and Visual Science*, *57*(9), OCT1-OCT13. doi: https://doi.org/10.1167/iovs.16-19963

Kapoor, R., Whigham, B. T., & Al-Aswad, L. A. (2019). Artificial intelligence and optical coherence tomography imaging. *The Asia-Pacific Journal of Ophthalmology*, *8*(2), 187-194. doi: 10.22608/APO.201904

Kim, S., Crose, M., Eldridge, W. J., Cox, B., Brown, W. J., & Wax, A. (2018). Design and implementation of a low-cost, portable OCT system. *Biomedical Optics Express*, *9*(3), 1232-1243. doi: https://doi.org/10.1364/BOE.9.001232

Lee, S. S., Song, W., & Choi, E. S. (2020). Spectral domain optical coherence tomography imaging performance improvement based on field curvature aberration-corrected spectrometer. *Applied Sciences, 10*(10), 1-15. doi: https://doi.org/10.3390/app10103657

Lee, S. W., Song, H. W., Kim, B. K., Jung, M. Y., Kim, S. H., Cho, J. D., & Kim, C. S. (2011). Fourier domain optical coherence tomography for retinal imaging with 800-nm swept source: Real-time resampling in k-domain. *Journal of the Optical Society of Korea*, *15*(3), 293-299.

Lee, W. D., Devarajan, K., Chua, J., Schmetterer, L., Mehta, J. S., & Ang, M. (2019). Optical coherence tomography angiography for the anterior segment. *Eye and Vision, 6*(1), 1-9. doi: https://doi.org/10.1186/s40662-019-0129-2

Liu, J., Zhu, J., Zhu, L., Yang, Q., Fan, F., & Zhang, F. (2020). Quantitative assessment of optical coherence tomography angiography algorithms for neuroimaging. *Journal of Biophotonics*, *13*(9), 1-9. doi: https://doi.org/10.1002/jbio.202000181

Marks, D. L., Oldenburg, A., Reynolds, J. J., & Boppart, S. A. (2002, July 7-10). Digital dispersion compensation in optical coherence tomography. In *Proceedings IEEE International Symposium on Biomedical Imaging* (pp. 621-624). Washington, DC, USA. doi: 10.1109/ISBI.2002.1029334

McKeown, M. (2010). *FFT Implementation on the TMS320VC5505, TMS320C5505, and TMS320C5515 DSPs* (SPRABB6B). Application report, Texas instruments. Retrieved October 9, 2020, from https://www.ti.com/lit/an/sprabb6b/sprabb6b.pdf?ts=1606467818116&ref_url=https%253A%252F%252Fwww.google.com%252F

Murakami, T., & Ogawa, K. (2018, March 9-10). Speckle noise reduction of optical coherence tomography images with a wavelet transform. In *2018 IEEE 14th International Colloquium on Signal Processing & Its Applications (CSPA)* (pp. 31-34). Batu Feringghi, Malaysia. doi: 10.1109/CSPA.2018.8368680

Panta, P., Lu, C. W., Kumar, P., Ho, T. S., Huang, S. L., Kumar, P., ... & John, R. (2019). Optical coherence tomography: Emerging *in vivo* optical biopsy technique for oral cancers. In P. Panta (ed.), *Oral Cancer Detection* (pp. 217-237). Cham, Switzerland: Springer. doi: https://doi.org/10.1007/978-3-319-61255-3_11

Patil, K., Mahajan, A., Balamurugan, S., Arulmozhivarman, P., & Makkar, R. (2020, July 28-30). Development of signal processing algorithm for optical coherence tomography. In *2020 International Conference on Communication and Signal Processing (ICCSP)* (pp. 1283-1287). Chennai, India. doi: 10.1109/ICCSP48568.2020.9182121

Petrov, D. A., Abdulkareem, S. N., Ghaleb, K. E., & Proskurin, S. G. (2016). An improved algorithm of structural image reconstruction with rapid scanning optical delay line for optical coherence tomography. *Journal of Biomedical Photonics and Engineering*, *2*(2), 1-6.

Rawat, C. S., & Gaikwad, V. S. (2014, July 10-11). Signal analysis and image simulation for optical coherence tomography (OCT) systems. In *2014 International Conference on Control, Instrumentation, Communication and Computational Technologies (ICCICCT)* (pp. 626-631). Kanyakumari, India. doi: 10.1109/ICCICCT.2014.6993037

Schönfeldt-Lecuona, C., Kregel, T., Schmidt, A., Kassubek, J., Dreyhaupt, J., Freudenmann, R. W., ... & Pinkhardt, E. H. (2020). Retinal single-layer analysis with optical coherence tomography (OCT) in schizophrenia spectrum disorder. *Schizophrenia Research*, *219*, 5-12. doi: https://doi.org/10.1016/j.schres.2019.03.022

Tang, S. N., Hsiang, C. Y., & Huang, S. J. (2018, June 25-29). Hardware/software codesign for portable optical coherence tomography (OCT) applications. In *2018 Joint 7th International Conference on Informatics, Electronics & Vision (ICIEV) and 2018 2nd International Conference on Imaging, Vision & Pattern Recognition (icIVPR)* (pp. 24-28). Kitakyushu, Japan. doi: 10.1109/ICIEV.2018.8641052

Tomlins, P. H., & Wang, R. K. (2005). Theory, developments and applications of optical coherence tomography. *Journal of Physics D: Applied Physics*, *38*(15), 2519-2535. doi: https://doi.org/10.1088/0022-3727/38/15/002

Zhang, Q., Zheng, F., Motulsky, E. H., Gregori, G., Chu, Z., Chen, C. L., & Wang, R. K. (2018). A novel strategy for quantifying choriocapillaris flow voids using swept-source OCT angiography. *Investigative Ophthalmology & Visual Science*, *59*(1), 203-211. doi: https://doi.org/10.1167/iovs.17-22953